The manuscript reports on the MJO simulation by two versions of the IFS-NEMO model configured at two horizontal resolutions: 9 km and 25 km. The manuscript is well written. The diagnostics applied to evaluate the MJO characteristics simulated by the model are described in detail, which makes the analysis easy to follow. There are only a few minor changes that need to be implemented:

L37: Maloney and Hartmann (2001) was the first study investigating the relationship between MJO and TCs. Reference added in the text and bibliography.

L175: Waliser (2009) applies a 20-100 day filter whereas Kim et al. (2025) apply a 20-70 filter. Since one of the objectives of the paper is to also conduct sensitivity tests (e.g., OLR from NOAA satellite data set and ERA 5, reconstruction of anomalies, propagation speed), the authors should also consider evaluating the sensitivity of analysis to the filtering window.

Thank you for addressing this point. Sensitivities tests were indeed conducted by the authors, though they were not reported in the submitted version of the manuscript. We tested different combinations of filtering windows, using 20 or 30 days^{-1} for the low pass and 70, 80, 90 or 100 days^{-1} for the high pass (Fig. S5). Specifically, using the same 20-70 filter as Kim et al. (2025) yields results consistent with their work, with a propagation speed of 5.95 ms^{-1} in observations for OLR over the 1979-2014 period. IFS-NEMO-HR consistently shows a better propagation speed when compared to observations, although with generally much larger uncertainty and a less coherent propagation structure. IFS-NEMO-ER consistently underestimates the propagation speed but the signal propagation is more coherent than in IFS-NEMO-HR. We note that we also tested the sensitivity of the method proposed by Kim et al. (2025) to the correlation level chosen as boundary for the linear regression during the computation of the propagation speed (not shown here). Using the 0.2 correlation threshold yields qualitatively similar results to the use of the 0.3 level. Increasing the threshold to 0.4 preserves the comparison between IFS-NEMO-ER and ERA5, while it prevents the retrieval of a meaningful propagation speed for IFS-NEMO-HR, due to its less coherent signal structure. The figure illustrating the sensitivity of the filtering to the propagation speed has been added to the Supplementary material. We also note that, when recomputing the plots for the sensitivity test we noticed an error in the lag-correlation computation script. The figure has been corrected in the main manuscript and the discussion around it has been updated. This does not affect the main conclusions.

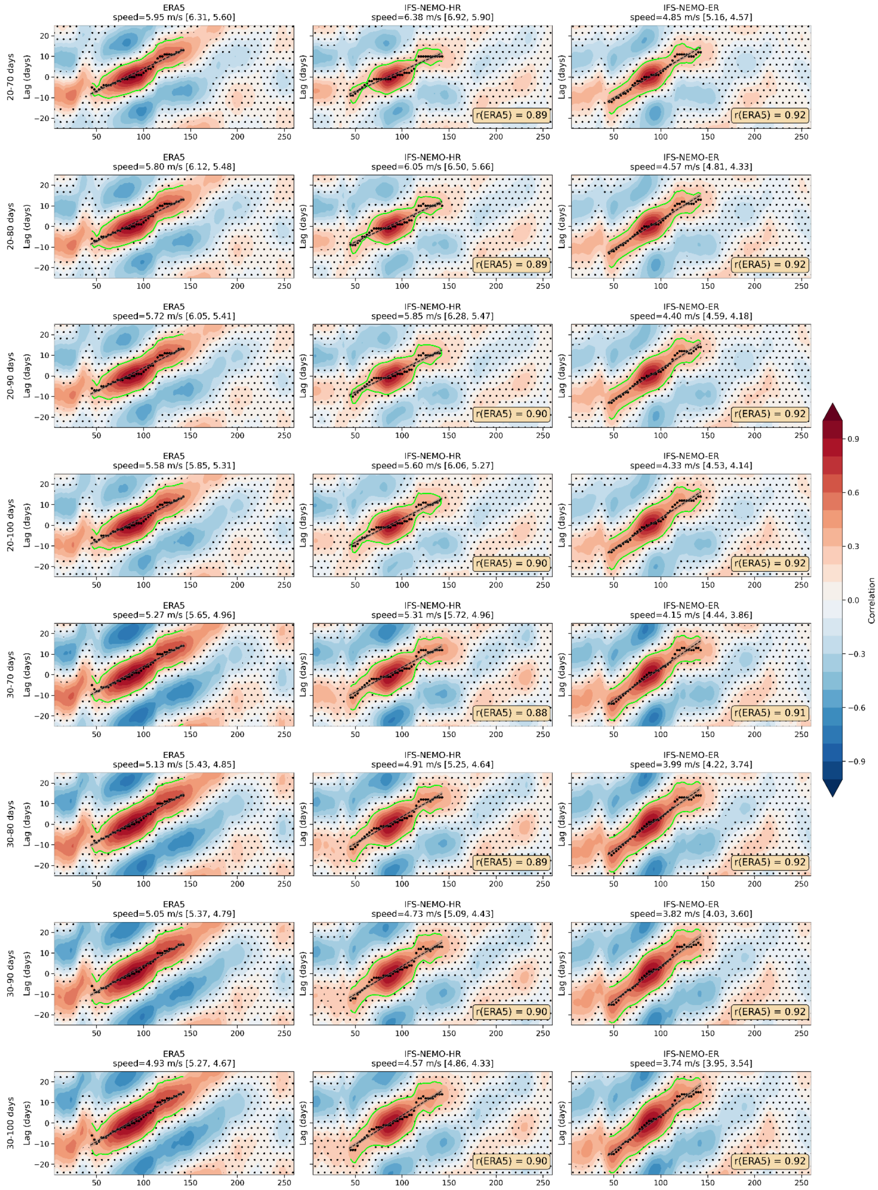

Figure S5: Sensitivity to the bandpass filter boundaries. Each panel shows lag - longitude maps of 15º S-10º N meridionally averaged OLR anomalies correlation against the Indian Ocean region (75º E-100º E) mean. The sensitivity test considered combinations of lower filtering boundaries of 20 and 30 days^{-1} and upper boundaries of 70, 80, 90, and 100 days^{-1}. Propagation velocities have been computed over the same longitudinal range for all cases considering correlation maxima within the 0.3 positive contour (in green), chosen as the minimal range over which all windows show correlation maxima.

L211: Something is missing after 96. Perhaps days? In parenthesis: 35=years, 365=days, Explain the meaning of 12. Changed in the text. We clarified the meaning of each number, as 96 was referring to the segment size chosen for the power spectra computation.

L212: Every step in the analysis is well justified, except the choice of dof=1000. How was this value selected? Were sensitivity tests conducted?

We thank the reviewer for this comment as this step is usually overlooked in literature when discussing the commonly used wavenumber-frequency power spectra. The choice of dof=1000 is a conservative estimate justified here, similarly to what was originally done by Wheeler and Kiladis (1999), by considering that the methodology does not take into account independent segments, and therefore using dof=1600 would be too optimistic. At the same time, we note that the methodology employed to compute the power spectra is not really sensitive to the choice of dof. In fact, because the spectra are derived by removing (dividing by) a background red noise spectrum, the power peaks above 1 already refer to significant signals. This can easily be tested by computing the 95% significance level of an F distribution for different dof, which do not affect the results shown in Fig. 4.

L265: The variance explained is shown in Table 1.

Changed in the text.

L321: Panels in Figure 4 show no dashed lines marking the MJO domain in the wavenumber frequency space.

The dashed lines have been removed from the figure for visual clarity as the relevant MJO domain is now better stated in the text. The caption has been updated.

Moist static energy (MSE) is a metric used to characterize the MJO amplitude. An elegant diagnostic explaining the amplitude of the MJO is the charged MSE introduced by Choi et al. (2026). This diagnostic would make a nice addition to the evaluation.

We thank the reviewer for the precious suggestion. The additional analysis turned out to support our previous conclusions, and adds a new physical perspective to the discussion which highlights the merits of the increased resolution as well as the biases shared by the two versions of IFS-NEMO. We note that this part of the analysis so far only covers the period 1990–2010 because we are facing some internal problems to download the required data for ERA5, which is progressing slowly. Once all data from ERA5 is recovered, which we expect to happen in the next 3 weeks, we will update the computation so we can include the revised results in the new version of the manuscript. We also note that, since IFS-NEMO does not archive all the fields required to explicitly diagnose the MSE tendency through a full budget analysis, we instead approximate it by computing the forward finite difference of MSE at each time step. This procedure prevents a complete decomposition of the MSE tendency budget but produces reasonable results.

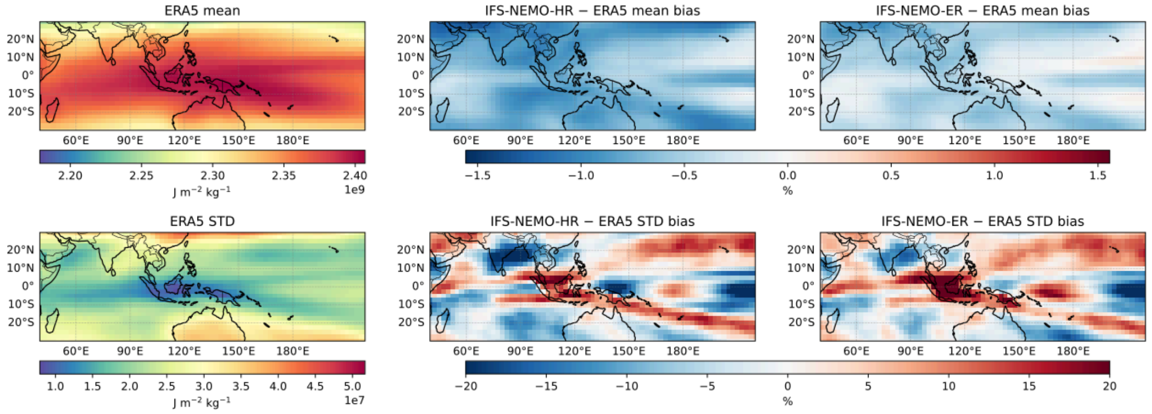

New Figure 7: Vertically integrated Moist Static Energy (MSE) climatological mean (top) and variability (bottom) in ERA5, with the corresponding IFS-NEMO-HR and IFS-NEMO-ER biases. The variability is computed as the standard deviation of the vertically integrated MSE

Following the approach of Choi et al. (2026) vertically integrated moist static energy (MSE) has been computed for ERA5 and IFS-NEMO-HR/ER. Figure S6a,c reveals that IFS-NEMO represents quite well the climatological MSE, with a reduction of the bias when increasing the resolution from 25 km to 9 km. As highlighted by the work of Choi et al. (2026), a good representation of the MSE mean state is not sufficient to ensure a good model performance in terms of MJO activity. We found that IFS-NEMO-HR highly overestimates the MSE variability in time (MSE standard deviation) over the maritime continent. Increasing the horizontal resolution seems to increase the variability even more over the maritime continent with respect to ERA5. Additionally, by analysing the charged MSE over the Indian Ocean and the Western Pacific regions, we find that IFS-NEMO underestimates the total energy available to generate deep convection associated with the MJO (with IFS-NEMO-ER slightly alleviating this bias). This deficiency is linked to the underestimation of the MJO activity in the model while the overestimation of MSE variability over the MC, exacerbated in IFS-NEMO-ER, contributes to the MC continent barrier in the model.

These figures and results are now included and discussed in the manuscript.

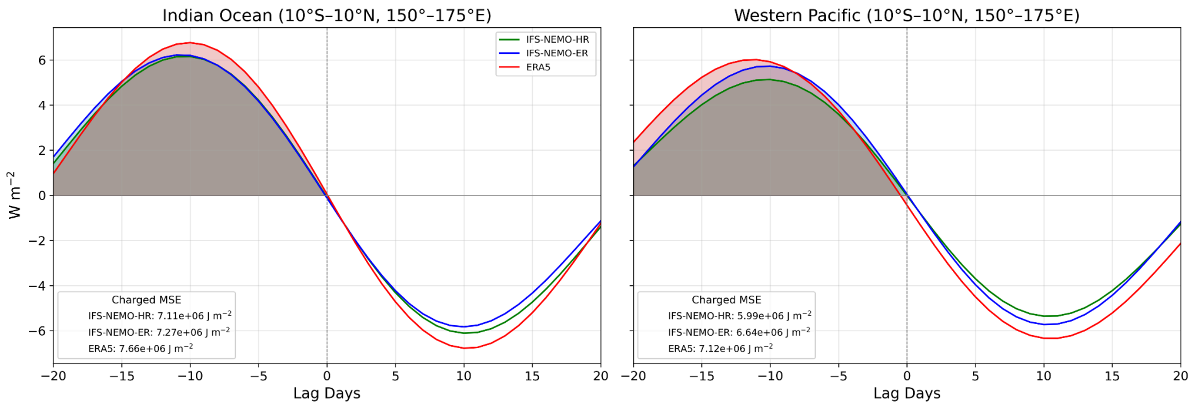

New Figure 8: The lag-regression between the MSE tendency and the total MSE over the Indian Ocean (10ºS, 10ºN; 75-100 ºE) and the Western Pacific (10ºS, 10ºN, 150-175 ºE). The charged MSE is computed as the integral of the MSE tendency for negative lags.

L573-574: Results from simulation using the super-parameterization confirmed that cloud -permitting schemes for moist convection alleviate this bias (e.g., Thayer-Calder and Randall, 2009; Stan et al., 2010)

We have added this reference to the discussion

Figure 8: Add labels to every panel and include a reference to the specific panel in the text when discussing them.

Labels have been added to each panel of the figure.

The variances shown in Figure 8 are consistent with the power spectrum in Figure 4. It would be interesting to compare the spectra for the earlier period when there is a better agreement between ERA5 and the models. That comparison can be added to the supplemental materials.

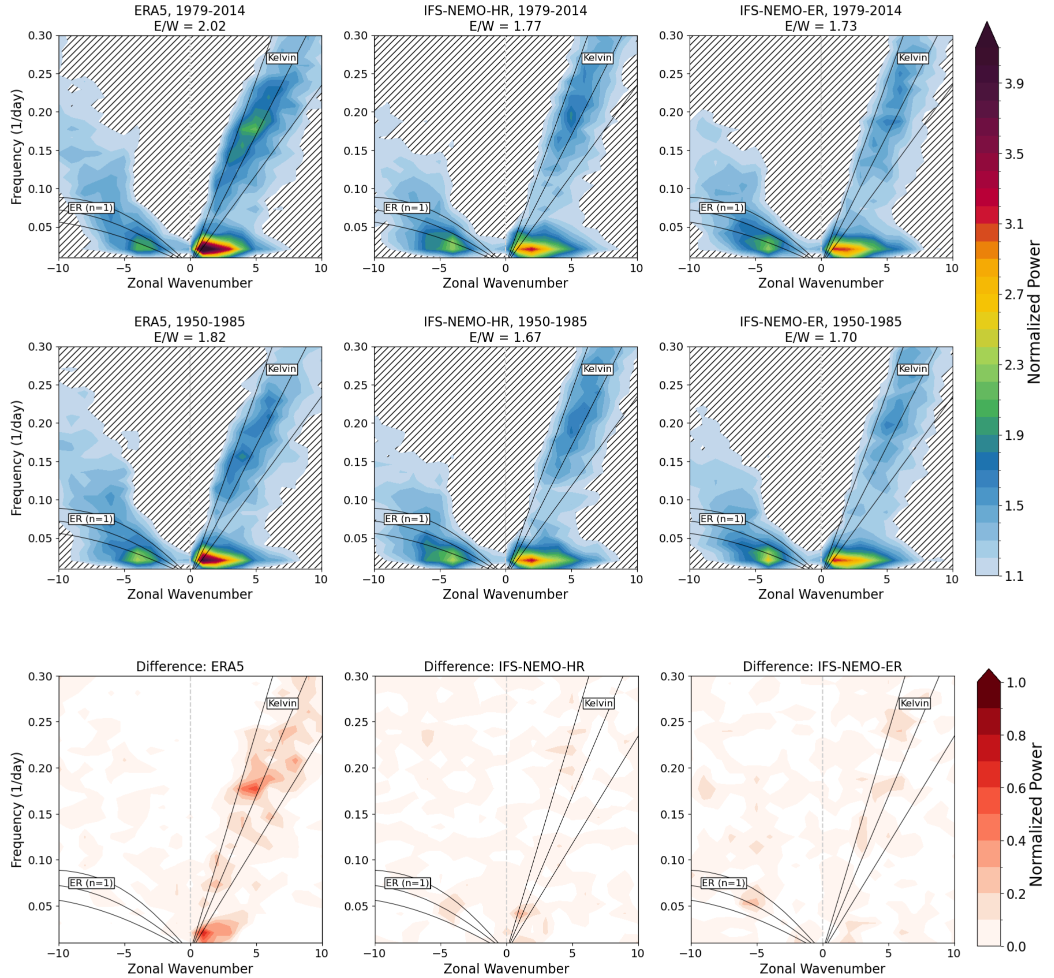

Figure S6: Wavenumber-frequency power spectra as shown in Fig. 4 using ERA5 as a reference instead of satellite observations during 1979-2014 (a) and 1950-2015 (b). Each of the power spectra has been computed separately, following the procedure described in *Methods.* (c) shows the difference between the 2 periods.

We thank the reviewer for suggesting this addition to the analysis. The comparison of power spectra between the 1979-2014 and the 1950-1985 periods is consistent with the results of Fig. 8. Specifically, the MJO-related variance in IFS-NEMO is in better agreement with ERA5 over the earlier period, although the model still under-represents the convective activity. We also note that during 1950-1985 IFS-NEMO simulates an improved E/W ratio and displays comparable Kelvin wave representation with ERA5. Figure S6 also confirms the difficulties of the model in capturing the observed long-term increase in MJO activity: the E/W ratio increase in IFS-NEMO-HR is halved with respect to ERA5, while in IFS-NEMO-ER the change is negligible. We note that this is consistent with Fig. 8a even if no long term change in MJO-variance is found in IFS-NEMO-HR. OLR is indeed the variable contributing the least to the EOF analysis employed to compute the MJO-variance. Thus, the relatively small long term increase in MJO activity observed in the IFS-NEMO-HR power spectra is outweighed by the long term changes in the intraseasonal circulation anomalies, as further discussed in section 3.2.

Maloney, E. D., and D. L. Hartmann, 2001: The Madden–Julian Oscillation, Barotropic Dynamics, and North Pacific Tropical Cyclone Formation. Part I: Observations. *J. Atmos. Sci.*, **58**, 2545–2558, https://doi.org/10.1175/1520-0469(2001)058<2545:TMJOBD>2.0.CO;2.

Choi, N., J. Stanczak, and C. Stan, 2026: The Role of Atmosphere–Ocean Coupling on the Prediction of Madden–Julian Oscillation. *J. Climate*, **39**, 3669–3684, https://doi.org/10.1175/JCLI-D-25-0247.1.

Thayer-Calder, K., and D. A. Randall, 2009: The Role of Convective Moistening in the Madden–Julian Oscillation. *J. Atmos. Sci.*, **66**, 3297–3312, https://doi.org/10.1175/2009JAS3081.1.

Stan, C., Khairoutdinov, M., C.A. DeMott, V. Krishnamurthy, D.Straus, D.A Randall, J. L. Kinter, and J Shukla, 2010: An ocean-atmosphere climate simulation with an embedded cloud resolving model. Geophysical Research Letters, 37, https://doi.org/10.1029/2009GL040822.
Citation: https://doi.org/10.5194/egusphere-2026-3251-RC1